Electronic Supplementary Information

Metal Organic Framework sensors on flexible substrate for ammonia sensing application at room temperature

Hugo Spieser[a, b], *Zari Tehrani**[b, c], *Muhammad Ali*[c], *Ehsaneh Daghigh Ahmadi*[c], *Aurore Denneulin*[a], *Julien Bras*[a,d], *Davide Deganello*[b], *David Gethin*[b]

[a] Univ. Grenoble Alpes, CNRS, Grenoble INP[e], LGP2, F-38000 Grenoble, France

[b] Welsh Centre for Printing and Coating, College of Engineering, Swansea University, Swansea, SA1 8EN, UK

[c] Centre for NanoHealth, College of Engineering, Swansea University, Swansea, SA2 8PP, UK

[d] Nestle Research Center, 1000 Lausanne, Switzerland

[e] Institute of Engineering Univ. Grenoble Alpes

Table SI 1. Summary of screen specifications used for screen-printing of the silver interdigitated electrode

Mesh count (threads per cm)	120
Wire diameter (µm)	34
Emulsion over mesh (OEM) thickness (µm)	12
Screen angle (°)	22.5

Table SI 2. Summary of the composition of the different CuBTC/carbon-graphene ink formulations for 1 mL of butyl acetate solvent

Formulation name (PGrCuBTC) %	Carbon-Graphene (mg)	CUBTC MOF (mg)
0 (control): CuBTC	0	200
20	50.0	200
21.25	54.0	200
22.5	58.1	200
25	66.7	200
30	85.7	200
50	200	200
100 (control): carbon/graphene ink	54	0

Gas sensing equipment:

The gas sensing system was built up using Sandvik 3R60 tubes with 6.25 x 0.89 mm 1/4" x20 dimensions and a flow chart of the whole system is displayed in **Figure SI 1.** Basically, the gas bottles were connected to ASCO (UK) SCG256B404VMS solenoid valves in order to close and open the desired section of the system. The lines were then connected to GFC17 mass flow controller (MFC) from Aalborg in order to control the desired flow of gas inside the lines. The different lines then meet in the gas chamber and the gases are extracted through an exhaust line.

In order to prepare the printed sensors for the gas sensing experiments, the following procedure was conducted. Crocodile clip connectors 65801-005LF from Farnell were clipped through the printed silver pads on the devices. Classic electrical wires were soldered onto in the crocodile clips and the other end was soldered on the metal connection of the feedthrough. Pictures of the prepared devices can be seen in **Figure SI 2**.

The sensor was placed in the gas flow and connected via the feedthrough to a Keithley 6487 meter which measure the resistance set to a resolution of 0.01 Ohm. The system is fully automated and it is possible to program different sensing steps and to control the following parameters: opening and closing of the relays, flow rate of the MFC and acquisition time.

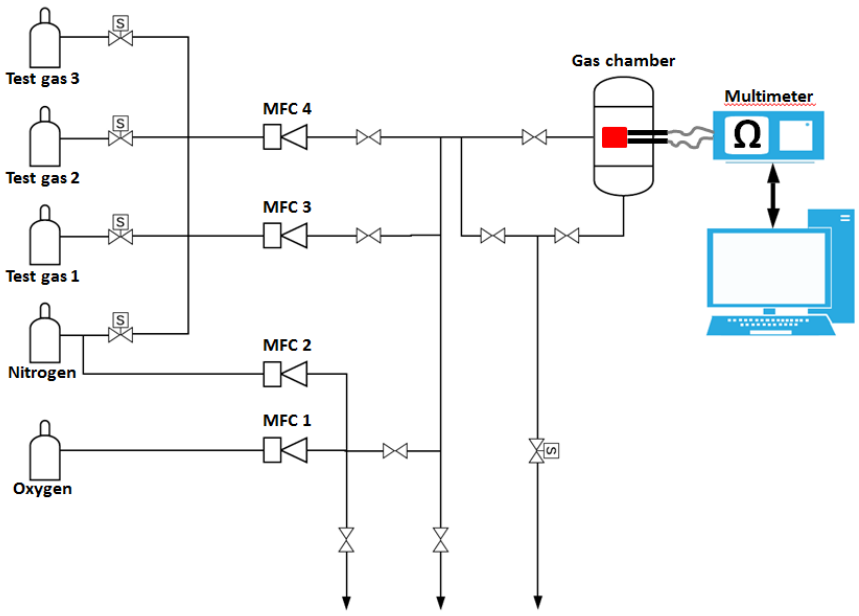

Figure SI 1. Schematic flow chart system of the custom-built gas rig system used for ammonia sensing

Figure SI 2. Picture of the printed sensors with connection for gas sensing (crocodile clips and soldered electrical wires) and the whole system soldered on the gas chamber feedthrough

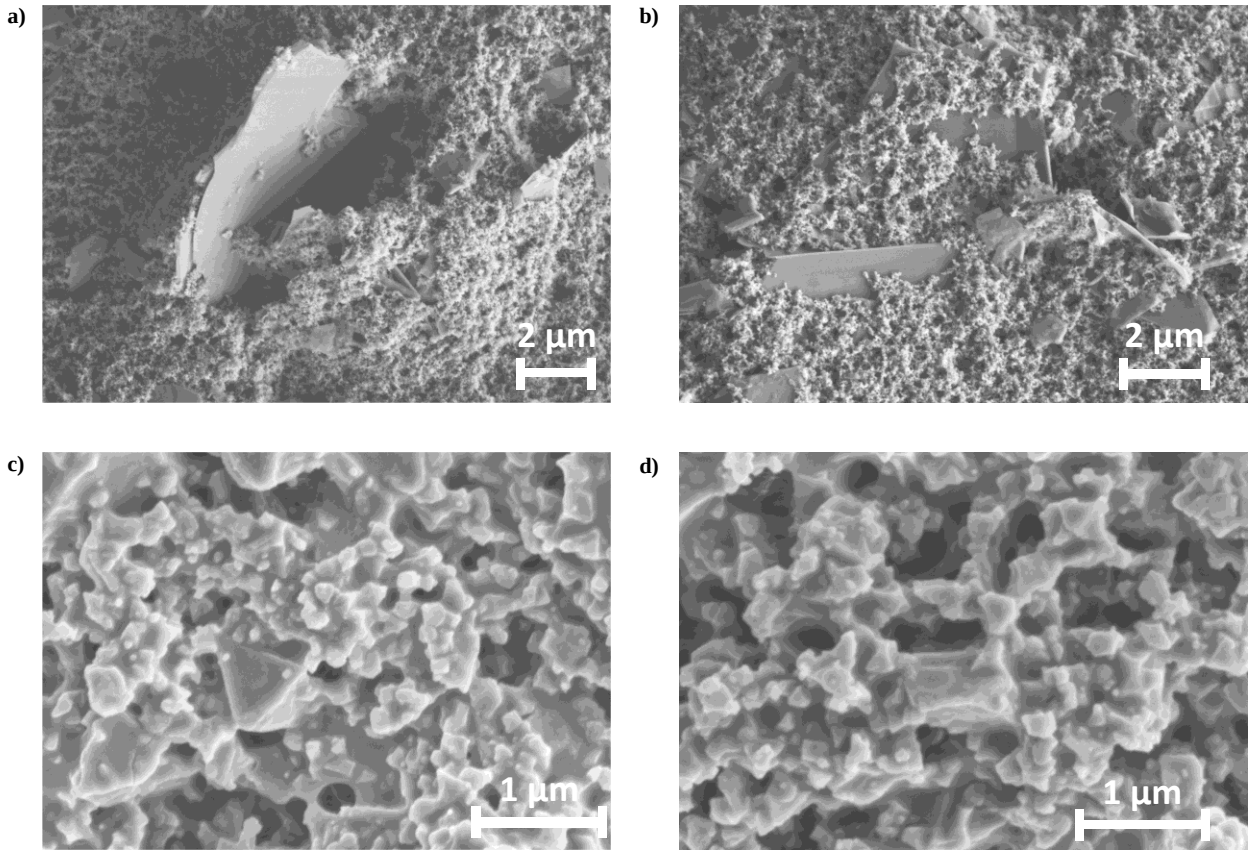

Figure SI 3. 2 SEM pictures of the surface of PGrCuBTC 100 with a) and b), and 2 SEM pictures of the surface of PGrCuBTC 0 with c) and d).

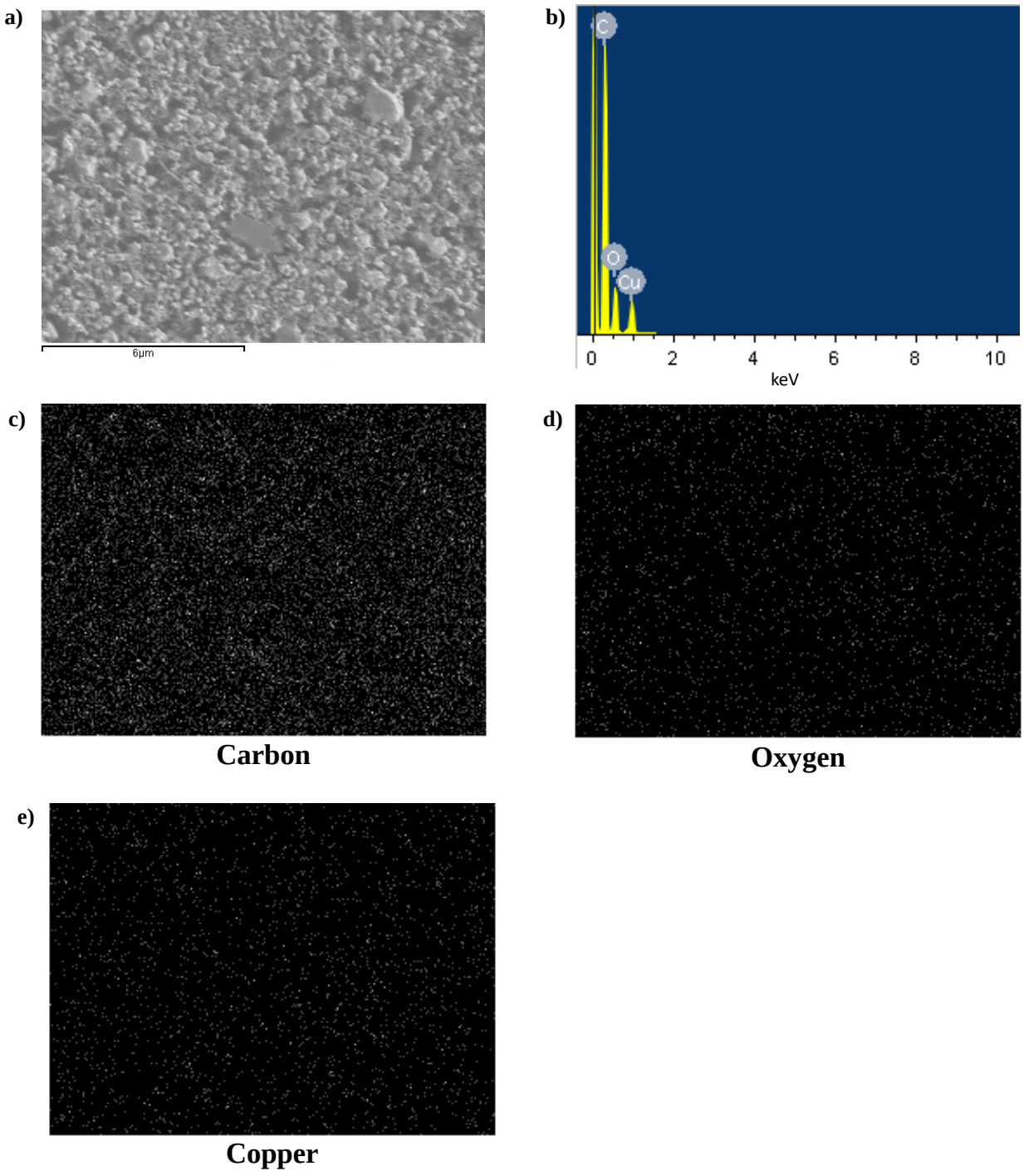

Figure SI 4: SEM-EDX of the surface of PGrCuBTC 21.25 with a) corresponding SEM image, b) recorded EDX spectrum c) mapping for carbon, d) mapping for oxygen and e) mapping for copper

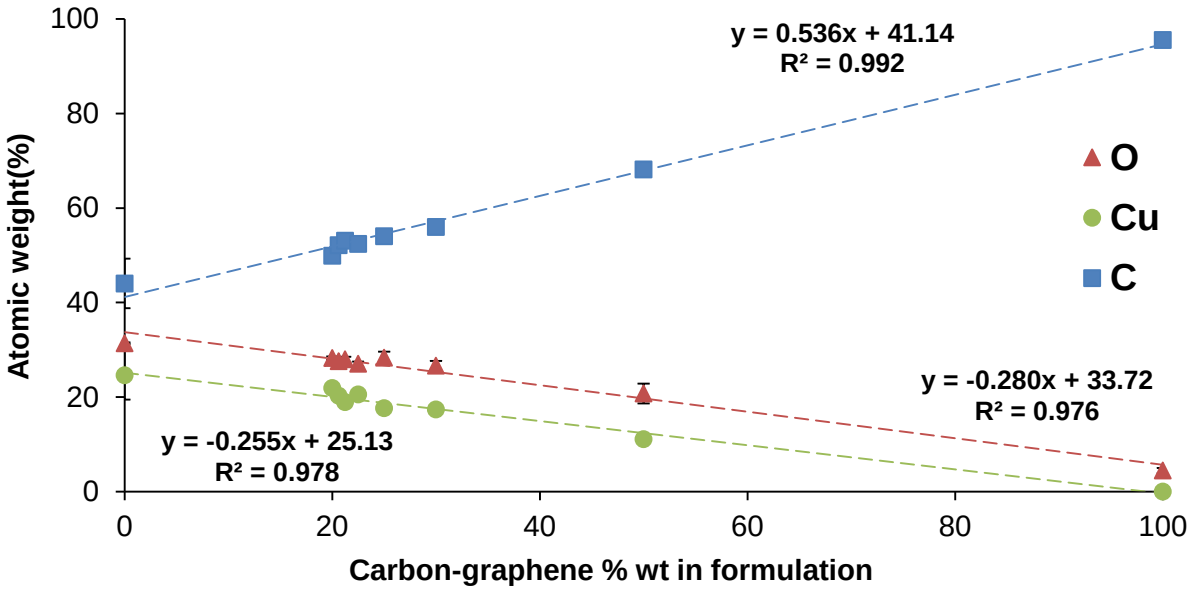

Figure SI 5: Atomic weight (%) for carbon, oxygen and copper atoms extracted from SEM-EDX mapping, compared to the mass percentage of carbon-graphene in the ink formulation

Table SI 3. Elemental concentration (atomic %) measured by X-ray photoelectron spectroscopy (XPS) for PGrCuBTC 100, 0 and 21.25

Sample name	Element	Atomic Concentration (%)
PGrCuBTC 100	O 1s	17.48 ± 0.14
	N 1s	2.02 ± 0.08
	C 1s	78.33 ± 0.16
	Cl 2p	2.17 ± 0.02
PGrCuBTC 0	Cu 2p	6.18 ± 0.04
	O 1s	33.73 ± 0.14
	N 1s	1.33 ± 0.21
	C 1s	58.58 ± 0.18
	Cl 2p	0.18 ± 0.04
PGrCuBTC 21.25	Cu 2p	2.48 ± 0.03
	O 1s	27.50 ± 0.14
	N 1s	1.02 ± 0.19
	C 1s	66.54 ± 0.20
	Cl 2p	2.46 ± 0.04

Table SI 4. Peak attribution and corresponding bonding energy position (eV) and atomic concentration (%) measured by X-ray photoelectron spectroscopy (XPS) for PGrCuBTC 100.

PGrCuBTC 100			
Element	**Component**	**Binding Energy Position (eV)**	**Atomic Conc. (%)**
C1s	C=C	284.09	59.58
	C-C	284.89	6.55
	C-O, (C-N)	286.33	26.85
	C=O, (C=N)	288.28	5.38
	O-C=O, (O-C-O), (N-C=O)	290.40	1.64
N1s	Nitrate	407.29	100.00
O1s	C=O	531.98	25.76
	C-O	533.08	35.35
	NO_3	533.47	38.88

Table SI 5. Peak attribution and corresponding bonding energy position (eV) and atomic concentration (%) measured by X-ray photoelectron spectroscopy (XPS) for PGrCuBTC 0.

PGrCuBTC 0			
Element	**Component**	**Binding Energy Position (eV)**	**Atomic Conc. (%)**
C1s	C-C	284.79	57.32
	C-O, (C-N)	286.57	19.12
	C=O, (C=N)	288.61	21.09
	O-C=O, (N-C=O)	290.59	2.47
N1s	Nitrate	407.81	68.24
	Amine	400.53	31.76
O1s	CuO	531.00	5.77
	C=O	531.70	42.41
	C-O	532.73	32.80
	NO_3	533.83	19.02
Cu 2p	Cu^+, Cu(0)	932.88	14.01
	Cu^{2+}	934.73	26.35
	Cu^{2+} Satellite	939.77	15.53
	Cu^{2+} Satellite	942.41	3.01
	Cu^{2+} Satellite	944.32	11.00
	Cu^+, Cu(0)	952.67	8.63
	Cu^{2+}	954.57	10.08
	Cu^{2+} Satellite	959.57	4.57
	Cu^{2+} Satellite	961.22	0.88
	Cu^{2+} Satellite	963.16	5.94

Table SI 6. Peak attribution and corresponding bonding energy position (eV) and atomic concentration (%) measured by X-ray photoelectron spectroscopy (XPS) for PGrCuBTC 21.25

PGrCuBTC 21.25			
Element	**Component**	**Binding Energy Position (eV)**	**Atomic Conc. (%)**
C1s	C=C	284.00	24.73
	C-C	284.63	33.40
	C-O, (C-N)	286.17	23.59
	C=O, (C=N)	288.15	13.23
	O-C=O, (O-C-O), (N-C=O)	289.03	5.05
N1s	Nitrate	407.78	74.36
	Amine	400.52	25.64
O1s	CuO	531.17	3.25
	C=O	531.90	49.19
	C-O	533.21	32.80
	NO_3	534.23	14.76
Cu 2p	Cu^+, Cu(0)	932.56	10.60
	Cu^{2+}	934.45	29.47
	Cu^{2+} Satellite	939.43	15.54
	Cu^{2+} Satellite	942.50	8.23
	Cu^{2+} Satellite	944.31	8.22
	Cu^+, Cu(0)	952.23	4.87
	Cu^{2+}	954.23	12.05
	Cu^{2+} Satellite	959.33	4.09
	Cu^{2+} Satellite	961.90	3.02
	Cu^{2+} Satellite	963.10	3.93

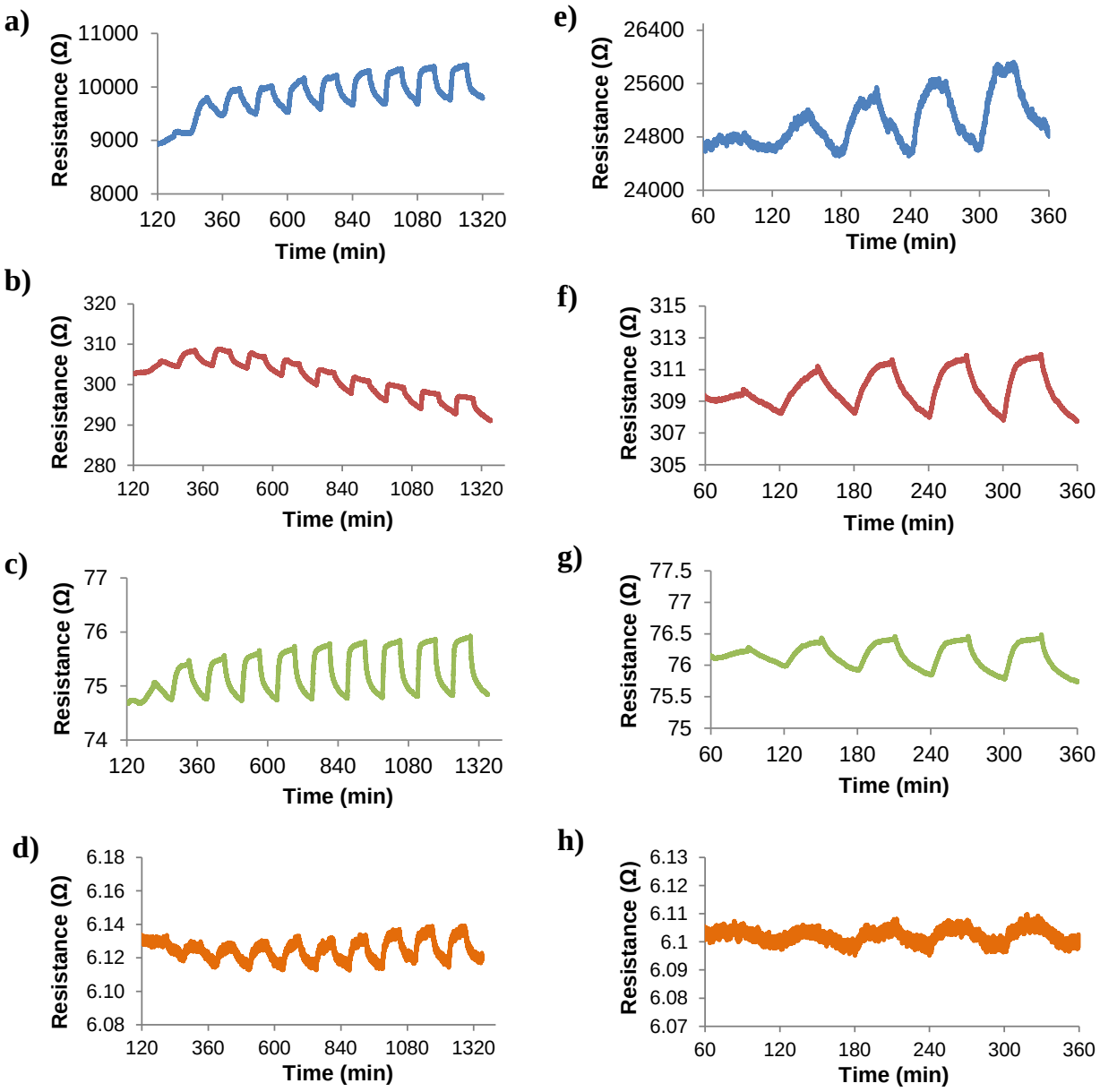

Figure SI 6. Gas sensing response of the sensors prepared with the different formulation when exposed to 50 to 500 ppm at a 50 ppm increment (High range) for a) PGrCuBTC 21.25, b) PGrCuBTC 22.5, c) PGrCuBTC 25, d) PGrCuBTC 100. Gas sensing response of the sensors prepared with the different formulation when exposed to 20 to 100 ppm at a 20 ppm increment (Low range) for e) PGrCuBTC 21.25, f) PGrCuBTC 22.5, g) PGrCuBTC 25, h) PGrCuBTC 100.

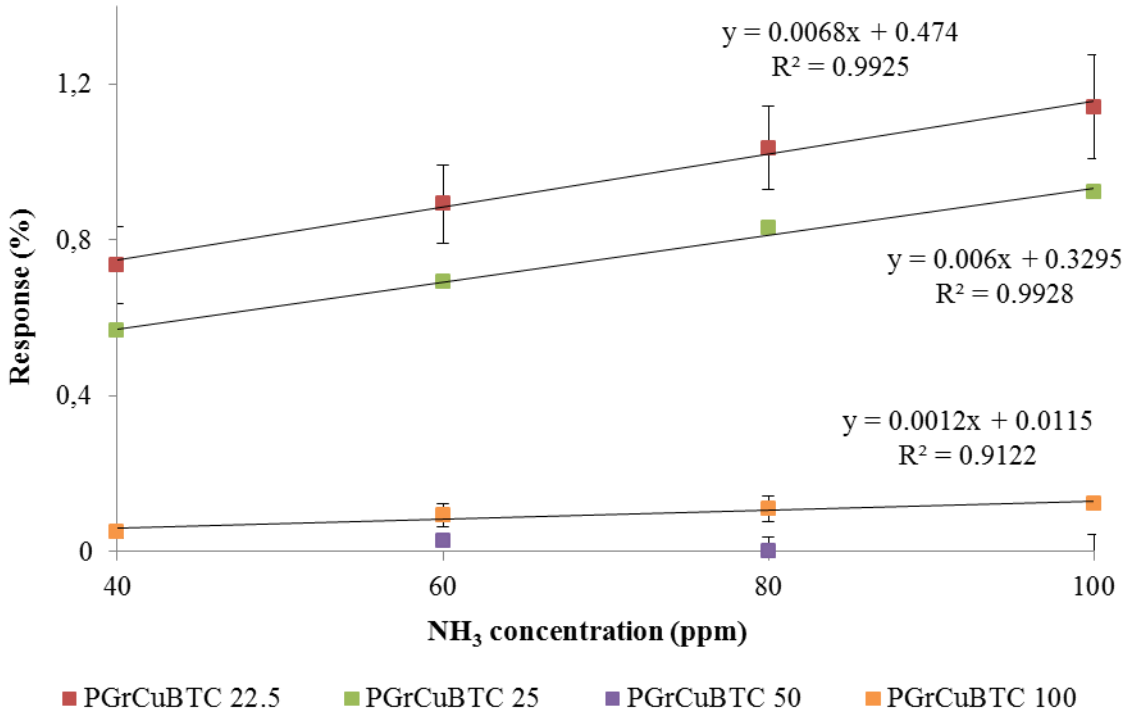

Figure SI 7. Summary of the gas sensing response (%) of PGrCuBTC 22.5, 25, 50 and 100 for 40-100 ppm range along with their linear fitting

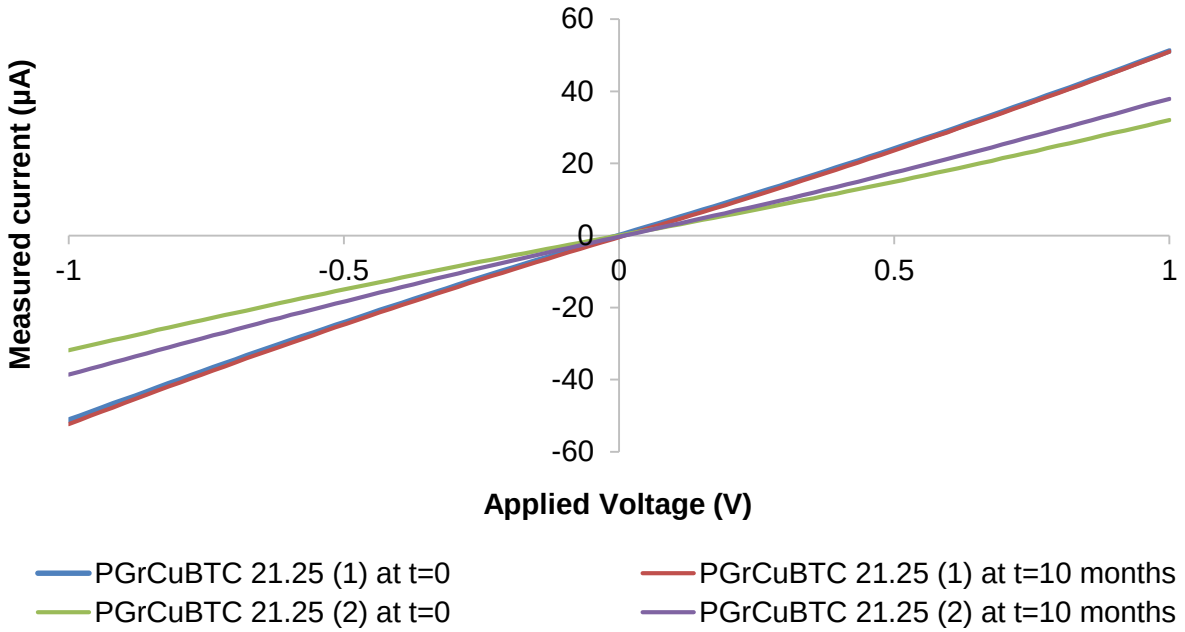

Figure SI 8. I/V measurement of two PGrCuBTC 21.25 devices (1 and 2) at t=0 and after 10 months of storage

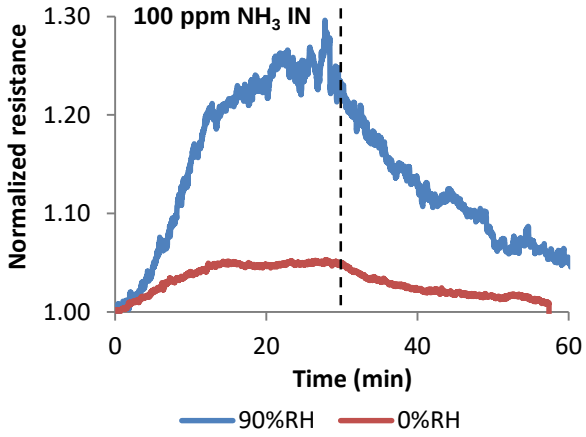

Figure SI 9. Humidity influence (approximatively 90% relative humidity, RH) on the PGrCuBTC 21.25 response (normalized resistance) against 100 ppm of NH_3, and comparison with the response under dry conditions.

Table SI 7. Literature review of ammonia sensing technology based on MOF: preparation, performances and operating parameters (NA= not applicable or not provided, App=approximate)

Sensor material	Sensing type	Device preparation (substrate)	Response (%, ppm)	Response calculation	Sensitivity (%.ppm^{-1})	Concentration range (ppm)	Response time/Recovery time (min)	Operating conditions	Commercial materials/ commercially available	reference
MOF										
$Cu_3(HITP)_2$	Conductance	Drop-casting suspension on Au IDE (NA)	0.81%/5 ppm 0.87%/5 ppm 0.70%/5 ppm 0.70%/5 ppm	$100*\Delta G/G_0$	App. 0.09	0.5-10	NA/NA	RT/dry N_2 RT/dry air RT/N_2 60%RH RT/air 60%RH	No/No	Campbell et al. 2015[1]
ZnO/ZIF-8 ZnO/ZIF-71	Conductance	Direct solvothermal growth (alumina ceramic)	37%/100 ppm 35%/100 ppm	$100*\Delta I/I_0$	App. 0.36 App. 0.33	10-200	NA/NA	250°C/dry air	No/Yes	Zhou et al. 2018[2]
$Cu_3(HHTP)_2$	Resistive	Spray layer-by-layer on Au IDE (glass)	129%/100 ppm	$100*\Delta R/R_0$	App. 1.03	1-100	1.36/9.11	RT/dry air	No/No	Yao et al. 2017[3]
SNNU-88	Resistive	Direct solvothermal growth on Ag-Pd IDE (ceramic)	2.3/50 ppm	R_0/R	1.29	5–100	1.45/2.12	25°C/air	No/No	Li et al. 2018[4]
ZIF8 Zn(INA) Zn(NA)	Resistive	Drop-casting suspension (glass)	9/100 ppm 139/100 ppm 220/100 ppm	R_0/R	App. 0.009 App. 2.41 App. 1.52	10-100	1.12/0.9 1.5/2.35 0.77/3.33	RT/dry air	No/Partially	Mohan et al. 2020[5]
Cu-TCPP on Cu-HHTP Zn-TCPP on Cu-HHTP	Resistive	layer by layer spray on Au IDE (sapphire)	70%/100 ppm 230%/100 ppm	$100*\Delta R/R_0$	App. 1.82 App. 2.13	1-100	NA/NA NA/NA	RT/dry air	No/No	Yao et al. 2019[6]
NiPc-Cu NiPc-Ni	Resistive	Drop-casting suspension on Au IDE	30%/80 ppm 14.5%/80 ppm	$100*\Delta G/G_0$	0.36 0.16	2-80	NA/NA	RT/dry N_2	No/No	Meng et al. 2019[7]
$Ba(o\text{-}CbPhH_2IDC)(H_2O)_4]_n$	Impedance	Pressed pellets	27%/25 ppm 148%/25 ppm 198%/25 ppm 243%/25 ppm	$100*\Delta Z/Z_0$	App. 0.95 App. 6.8 App. 8.5 App. 8.8	5-25	8/NA 10/NA 12/NA 13/NA	30°C/air 75%RH 30°C/air 85%RH 30°C/air 93%RH 30°C/air 98%RH	No/No	Guo et al. 2018[8]
$\{Na[Cd(MIDC)]\}_n$	Impedance	Pressed pellets	363%/30 ppm 662%/30 ppm 1379%/30 ppm	$100*\Delta Z/Z_0$	App. 46.7	0.05 -30	NA/NA NA/NA NA/NA	25°C/air 68%RH 25°C/air 85%RH 25°C/air 98%RH	No/No	Liu et al. 2018[9]
$[Cu(p\text{-}IPhHIDC)]_n$	Impedance	Pressed pellets	8620%/130 ppm 3900%/130 ppm 3231%/130 ppm 1824%/130 ppm 569%/130 ppm 484%/130 ppm	$100*\Delta Z/Z_0$	App. 69.95 App. 31.17 App. 25.96 App. 15.04 App. 3.42 App. 3.74	2-130	NA/NA NA/NA NA/NA NA/NA NA/NA NA/NA	25°C/air 68%RH 40°C/air 68%RH 25°C/air 85%RH 40°C/air 85%RH 25°C/air 98%RH 40°C/air 98%RH	No/No	Sun et al. 2018[10]
NDC-Y-fcu-MOF	Capacitive	Direct solvothermal growth on Au IDE (NA)	25%/100 ppm	$10^{-4}*100*\Delta C/C$	App. 0.24	1-100	4.17/NA	RT/dry N_2	No/No	Assen et al. 2017[11]
Eu^{3+}@Ga(OH)bpydc	luminescence	Suspension spin coating (quartz)	0.33/100 ppm	$1\text{-}I/I_0$	App. 0.001	10-500	NA/NA	RT/NH_3 [aq] vapor	No/No	Hao et Yan. 2016[12]
MIL-124@Eu3+	luminescence	Direct solvothermal growth (ceramic)	0.07/100 ppm	$1\text{-}I/I_0$	App. 0.0002	100-1350	NA/NA	0-60°C/air 0-100%RH	No/No	Zhang et al. 2017[13]

(continued)

Table SI 7. continued

[2]	Sensing type	Device preparation (substrate)	Response (%, ppm)	Response calculation	Sensitivity (%.ppm^{-1})	Concentration range (ppm)	Response time/Recover y time (min)	Operating conditions	Commercial materials/ commercially available	reference
FJU-56	Absorbance	MOF powder	1.051/10 ppm	A/A_0	App. 0.005	0-10	NA/NA	RT/NH_3 [aq] vapor	No/No	Zhang et al. 2018[14]
ZA-MPTMS-Eu-UiO-67	Fluorescence	Suspension precipitation (glass)	0.73/80 ppm	I/I_0	App. -0.003	40-200	NA/NA	RT/ NH_3 [aq] vapor	No/No	Ma et Yan 2019[15]
MR-MOF-Eu	Fluorescence	MOF deposition (glass)	0.75/100 ppm	I/I_0	App. -0.003	50-300	NA/NA	30C°C/NH_3 [aq] vapor	No/No	Ma et al. 2020[16]
MOF/Graphene										
Cu-BTC/graphite oxide	Resistive	Coating suspension on Au IDE (ceramic)	4/100 ppm	R/R_0	App. 0.008	100-500	NA/NA	RT/dry air	No/Yes	Travlou et al. 2015[17]
SiO_2 coated Cu-BTC/rGO/Pani	Resistive	Drop-casting suspension on 4 probe Cr electrode (NA)	144%/100 ppm	$100*\Delta R/R_0$	1.39	1-100	0.58/0.28	RT/NH_3 [aq] vapor	No/Yes	Bhardwaj et al. 2018[18]
Cu–BTC/PPy–rGO	Resistive	Drop-casting suspension on ITO substrate	12.4%/50 ppm	$100*\Delta R/R_0$	App. 0.15	10-150	0.22/0.27	25°C/air 50%RH	No/Yes	Yin et al. 2018[19]
Graphite/$Cu_3(HHTP)_2$ Graphite/$Co_3(HHTP)_2$ Graphite/$Fe_3(HHTP)_2$ Graphite/$Ni_3(HHTP)_2$	Conductance	Abrasion on Au IDE (paper)	4.6%/80 ppm 4.2%/80 ppm 4.0%/80 ppm 2.9%/80 ppm	$-100*\Delta G/G_0$	App. 0.07 App. 0.07 App. 0.08 App. 0.06	5-80	NA/NA NA/NA NA/NA	RT/dry N_2	No/No	Ko et al. 2017[20]
Cu-BTC/carbon-graphene	**Resistive**	**Drop-casting suspension on screen printed Ag IDE (PET)**	**4.6%/100ppm**	**$100*\Delta R/R_0$**	**0.054**	**20-100**	**12.86/22.95**	**RT/dry air**	**Yes/Yes**	**This study**

References

1 M. G. Campbell, D. Sheberla, S. F. Liu, T. M. Swager and M. Dincă, *Angewandte Chemie International Edition*, 2015, **54**, 4349–4352.

2 T. Zhou, Y. Sang, X. Wang, C. Wu, D. Zeng and C. Xie, *Sensors and Actuators B: Chemical*, 2018, **258**, 1099–1106.

3 M.-S. Yao, X.-J. Lv, Z.-H. Fu, W.-H. Li, W.-H. Deng, G.-D. Wu and G. Xu, *Angewandte Chemie International Edition*, 2017, **56**, 16510–16514.

4 Y.-P. Li, S.-N. Li, Y.-C. Jiang, M.-C. Hu and Q.-G. Zhai, *Chem. Commun.*, 2018, **54**, 9789–9792.

5 A. J. Mohan Reddy, N. K. Katari, P. Nagaraju and S. Manabolu Surya, *Materials Chemistry and Physics*, 2020, **241**, 122357.

6 M.-S. Yao, J.-W. Xiu, Q.-Q. Huang, W.-H. Li, W.-W. Wu, A.-Q. Wu, L.-A. Cao, W.-H. Deng, G.-E. Wang and G. Xu, *Angewandte Chemie International Edition*, 2019, **58**, 14915–14919.

7 Z. Meng, A. Aykanat and K. A. Mirica, *Journal of the American Chemical Society*, , DOI:10.1021/jacs.8b11257.

8 K. Guo, L. Zhao, S. Yu, W. Zhou, Z. Li and G. Li, *Inorg. Chem.*, 2018, **57**, 7104–7112.

9 R. Liu, Y. Liu, S. Yu, C. Yang, Z. Li and G. Li, *ACS Applied Materials & Interfaces*, , DOI:10.1021/acsami.8b18891.

10 Z. Sun, S. Yu, L. Zhao, J. Wang, Z. Li and G. Li, *Chemistry – A European Journal*, 2018, **24**, 10829–10839.

11 A. H. Assen, O. Yassine, O. Shekhah, M. Eddaoudi and K. N. Salama, *ACS Sens.*, 2017, **2**, 1294–1301.

12 J.-N. Hao and B. Yan, *Nanoscale*, 2016, **8**, 2881–2886.

13 J. Zhang, D. Yue, T. Xia, Y. Cui, Y. Yang and G. Qian, *Microporous and Mesoporous Materials*, 2017, **253**, 146–150.

14 J. Zhang, J. Ouyang, Y. Ye, Z. Li, Q. Lin, T. Chen, Z. Zhang and S. Xiang, *ACS Appl. Mater. Interfaces*, 2018, **10**, 27465–27471.

15 J. Ma and B. Yan, *Spectrochimica Acta Part A: Molecular and Biomolecular Spectroscopy*, 2019, **220**, 117107.

16 J. Ma, L.-M. Zhao, C.-Y. Jin and B. Yan, *Dyes and Pigments*, 2020, **173**, 107883.

17 N. A. Travlou, K. Singh, E. Rodríguez-Castellón and T. J. Bandosz, *J. Mater. Chem. A*, 2015, **3**, 11417–11429.

18 S. K. Bhardwaj, G. C. Mohanta, A. L. Sharma, K.-H. Kim and A. Deep, *Analytica Chimica Acta*, 2018, **1043**, 89–97.

19 Y. Yin, H. Zhang, P. Huang, C. Xiang, Y. Zou, F. Xu and L. Sun, *Materials Research Bulletin*, 2018, **99**, 152–160.

20 M. Ko, A. Aykanat, M. K. Smith and K. A. Mirica, *Sensors*, 2017, **17**, 2192.